Chemical Science

EDGE ARTICLE

View Article Online
View Journal | View Issue

Cite this: *Chem. Sci.*, 2016, **7**, 3820

A fascinating multifaceted redox-active chelating ligand: introducing the *N*,*N*′-dimethyl-3,3′-biquinoxalinium "methylbiquinoxen" platform†

Nicolas Leblanc,*[a] Stephen Sproules,[b] Karin Fink,[a] Lionel Sanguinet,[c] Olivier Alévêque,[c] Eric Levillain,[c] Patrick Rosa[d] and Annie K. Powell*[ae]

Received 19th December 2015
Accepted 24th February 2016

DOI: 10.1039/c5sc04904k

www.rsc.org/chemicalscience

To intimately combine a chelating ligand function with the numerous properties of a viologen-like redox-active centre would offer a rare possibility to design controllable multi-redox states, whose properties arise from strongly correlated phenomena between the organic ligand as well as with any metalloid coordinated centres. Such a concept previously proved to be feasible, however is not widely applicable owing to challenges in terms of synthesis, isolation, and aerial sensitivity of both the ligand and its metal complexes. Here we report the first stable example of such a redox-active molecule, *N*,*N*′-dimethyl-3,3′-biquinoxalinium$^{2+/\bullet+/0}$ "methylbiquinoxen, MBqn$^{2+/\bullet+/0}$", which shows a rich redox chemistry and chelates a metal ion in the case of the metal complex [$CdCl_2$(MBqn^0)]. This goes beyond what is possible to achieve using viologens, which are limited by not providing chelation as well as having no accessible biradicaloid state, corresponding to the neutral direduced MBqn^0 open-shell behaviour we observe here.

Introduction

Organic molecules with multiple oxidation levels accessed by electro-, photo-, or chemical means are of extreme importance in many biological, chemical and physical processes.[1–6] Among these, viologens, or *N*,*N*′-disubstituted-4,4′-bipyridinium (V^{2+}) species, have attracted most attention over the last 80 years. Acting as strong electron-acceptors, viologens undergo two reversible one electron reduction steps leading to a radical cation intermediate ($V^{\bullet+}$) and neutral form (V^0).[7,8]

The interest in viologen derivatives is motivated, amongst other things, by the ease of synthesis and tunability, the high degree of control concerning their reversible oxidation–reduction process, the range of colours from colourless (V^{2+}) to dark green/blue/purple ($V^{\bullet+}$), the paramagnetic nature of $V^{\bullet+}$, and their strong structural templating effects (V^{2+}).[9] These possibilities have led to their incorporation in a range of donor–acceptor complexes developed for various applications such as photo- and electrochromic displays,[10,11] charge accumulation,[12,13] fluorescence,[14,15] supramolecular host–guest complexes and molecular machines[4,16] as well as ferroelectrics.[17]

Research on viologens is mainly focused on two aspects. The first of these is the diversification of their properties achieved through incorporation of additional functions. The second aims to improve their longevity, in particular through improving the chemical and air stability of the radical intermediates. In this context, Kaim's group have replaced some carbon atoms with nitrogen atoms within the aromatic heterocycles, leading to a new type of redox-active ligand that intimately combines a viologen-like centre with the chelating function of 2,2′-bipyridine.[18–20] Despite an improved π-electron deficiency and an interesting coordination function that provides strong electronic coupling between the coordinated site (typically a metal ion) and the organic redox centre, synthetic challenges and persistent chemical and air instability, render these conceptually interesting molecules currently not useful for applications.

In the context of the potential for radical-based systems and the challenges to be addressed, we report here on the synthesis and characterization of a new stable reversible organic redox-active chelating ligand *N*,*N*′-dimethyl-3,3′-biquinoxalinium (MBqn^{2+}, $\mathbf{1}^{2+}$, Fig. 1 – grey), "methylbiquinoxen". In particular the dication $\mathbf{1}^{2+}$ and its monoprotonated direduced form (MBqn^0-H$^+$, $\mathbf{1}^0$-$\mathbf{H}^+$, Fig. 1 – purple) are thermally stable ($\mathbf{1}^{2+}$ and $\mathbf{1}^0$-$\mathbf{H}^+$ decomposes at $T \approx 500$ K and $T \approx 440$ K respectively, Fig. S2 and S4†), and neither moisture nor air-sensitive in the solid state even without complexation to a metal ion. As a consequence, BF_4^- salts of these can be prepared and handled

[a]*Institut für Nanotechnologie, Karlsruher Institut für Technologie, D-76344 Eggenstein-Leopoldshafen, Germany. E-mail: nicolas.leblanc@partner.kit.edu*
[b]*WestCHEM, School of Chemistry, University of Glasgow, Glasgow, G12 8QQ, UK*
[c]*Université d'Angers, CNRS UMR 6200, MOLTECH-Anjou, 2 bd Lavoisier, 49045 Angers Cedex, France*
[d]*Institut de Chimie de la Matière Condensée de Bordeaux CNRS, UPR 9048, 87 Avenue du Dr Albert Schweitzer, 33600 Pessac, France*
[e]*Institut für Anorganische Chemie, Karlsruher Institut für Technologie, Engesserstraße 15, D-76131, Karlsruhe, Germany. E-mail: annie.powell@kit.edu*

† Electronic supplementary information (ESI) available. CCDC 1043174, 1043175 and 1437399. For ESI and crystallographic data in CIF or other electronic format see DOI: 10.1039/c5sc04904k

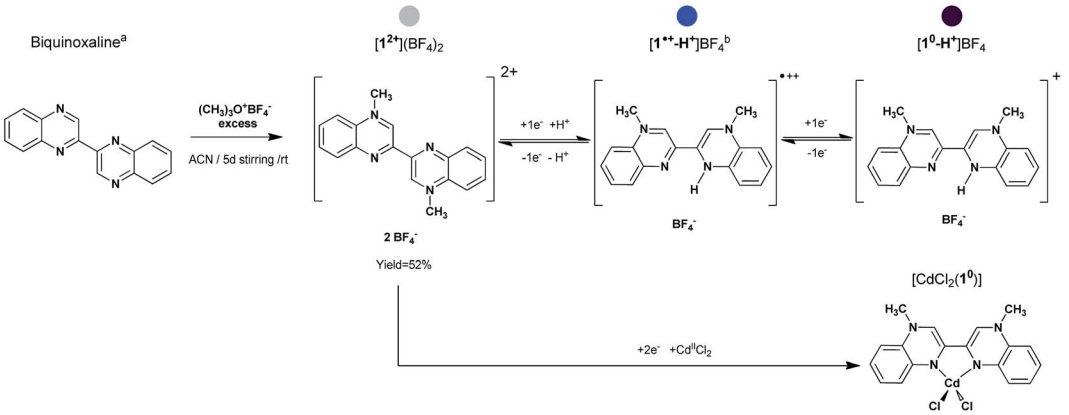

Fig. 1 Path for the synthesis of $[\mathbf{1}^{2+}](BF_4)_2$, $[\mathbf{1}^{0}\text{-}\mathbf{H}^{+}]BF_4$ and $[CdCl_2(\mathbf{1}^{0})]$. a = from ref. 21; b = $[\mathbf{1}^{\bullet+}\text{-}\mathbf{H}^{+}]BF_4$ not isolated in the solid state. The coloured stickers indicate the relative redox state of the methylbiquinoxen. Grey is for the dication, blue for the doublet radical, and purple for the direduced form.

as simple crystalline starting pro-ligands. A seemingly facile and reversible chemical reduction at room temperature leads to a doublet radical intermediate which is stable in solution under inert atmosphere (Fig. 1 – blue).

Using solvothermal conditions under inert atmosphere, the doubly reduced form MBqn^0 ($\mathbf{1}^{0}$) has been isolated in two crystalline forms, firstly as a cation in the monoprotonated species $[\mathbf{1}^{0}\text{-}\mathbf{H}^{+}]BF_4$ and secondly as a neutral biradicaloid chelating ligand in the metal complex $[CdCl_2(\mathbf{1}^{0})]$. Noteworthy is that dissolution of $[\mathbf{1}^{0}\text{-}\mathbf{H}^{+}]BF_4$ (Fig. 1 – purple) in DMF under inert atmosphere generates the same doublet radical species in solution (Fig. 1 – blue), thus granting the methylbiquinoxen three different accessible redox states which are chemically reversible (*vide infra*).

Both $\mathbf{1}^{2+}$ and $\mathbf{1}^{0}\text{-}\mathbf{H}^{+}$ have been characterized by X-ray diffraction analysis (single crystal, powder), UV-Vis-NIR, IR and mass spectrometry, thermogravimetric analysis, cyclic voltammetry, spectroelectrochemistry measurements, as well as DFT and TDDFT (Time Dependent Density Functional Theory) calculation. Additional SQUID, NMR and EPR studies of $\mathbf{1}^{0}\text{-}\mathbf{H}^{+}$ in the solid state (SQUID) and dissolved in DMF (SQUID, NMR, EPR) support the presence of the doublet radical intermediate species in solution.

Results and discussion

Synthetic procedures

General procedure for synthesis of compounds $[\mathbf{1}^{2+}](BF_4)_2$, $[\mathbf{1}^{0}\text{-}\mathbf{H}^{+}]BF_4$, and $[CdCl_2(\mathbf{1}^{0})]$ (Fig. 1). Compound $[\mathbf{1}^{2+}](BF_4)_2$ was obtained from Meerwein alkylation by mixing biquinoxaline[21] with an excess of trimethyloxonium tetrafluoroborate in acetonitrile. After 5 d stirring at room temperature, the resulting solid was isolated by filtration, washed with Et_2O, and recrystallized from water to give pale yellow/off-white crystals in 52% yield. Crystals of the direduced monoprotonated species $[\mathbf{1}^{0}\text{-}\mathbf{H}^{+}]BF_4$ as well as of the metal complex $[CdCl_2(\mathbf{1}^{0})]$ were obtained from solvothermal reaction using the solvent (here methanol) as the reducing agent. In a Schlenk tube, equipped with a hermetic Teflon stopper, $[\mathbf{1}^{2+}](BF_4)_2$ were mixed with a mixture of MeOH/DMF. The Schlenk was purged with nitrogen and inserted in a solvothermal oven to follow a heat/flat/cool temperature programme, resulting in a pure phase of dark purple crystals of $[\mathbf{1}^{0}\text{-}\mathbf{H}^{+}]BF_4$ in 68% yield. Phase purity of $[\mathbf{1}^{2+}](BF_4)_2$ and $[\mathbf{1}^{0}\text{-}\mathbf{H}^{+}]BF_4$ was checked by XRPD (Fig. S1 and S3†). For the synthesis of the cadmium complex the same precedent procedure was followed by adding a stoichiometric amount of $CdCl_2$ in the Schlenk tube. A violet crystal of $[CdCl_2(\mathbf{1}^{0})]$ was selected from a mixture of phases which always result from the reaction. In spite of many attempts it was only possible to generate the intermediate doublet radical species in solution, but not to isolate it as a crystalline salt.

Crystallography

Single crystals suitable for X-ray diffraction analysis were isolated for the dication $[\mathbf{1}^{2+}](BF_4)_2$ (Fig. 1 – grey) for the direduced monoprotonated form $[\mathbf{1}^{0}\text{-}\mathbf{H}^{+}]BF_4$ (Fig. 1 – purple) as well as for the metal complex $[CdCl_2(\mathbf{1}^{0})]$. A summary of the crystallographic

Table 1 Summary of crystallographic data for $[\mathbf{1}^{2+}](BF_4)_2$, $[\mathbf{1}^{0}\text{-}\mathbf{H}^{+}]BF_4$ and $[CdCl_2(\mathbf{1}^{0})]$

	$[\mathbf{1}^{2+}](BF_4)_2$	$[\mathbf{1}^{0}\text{-}\mathbf{H}^{+}]BF_4$	$[CdCl_2(\mathbf{1}^{0})]$
Fw (g mol^{-1})	461.97	376.16	471.85
Space group	$P\bar{1}$	$P2_1/n$	$P\bar{1}$
a, Å	7.5470(8)	7.1330(9)	7.4683(5)
b, Å	7.8860(7)	20.0360(16)	10.4739(7)
c, Å	8.9920(9)	11.5260(13)	11.3249(8)
α, °	66.005(7)	90	80.150(6)
β, °	85.305(8)	99.454(9)	82.274(5)
γ, °	83.508(8)	90	81.982(6)
V, Å^3	485.40(8)	1624.9(3)	858.70(10)
Z	1	4	2
T (K)	180	180	180
Obs. reflns ($I > 2\sigma(I)$) [R_{int}]	1527 [0.021]	2273 [0.042]	3386 [0.028]
No. of parameters	177	313	291
$R1(I > 2\sigma(I))$/w$R2$ (all data)	0.044/0.125	0.042/0.126	0.027/0.067
CCDC number	1043174	1043175	1437399

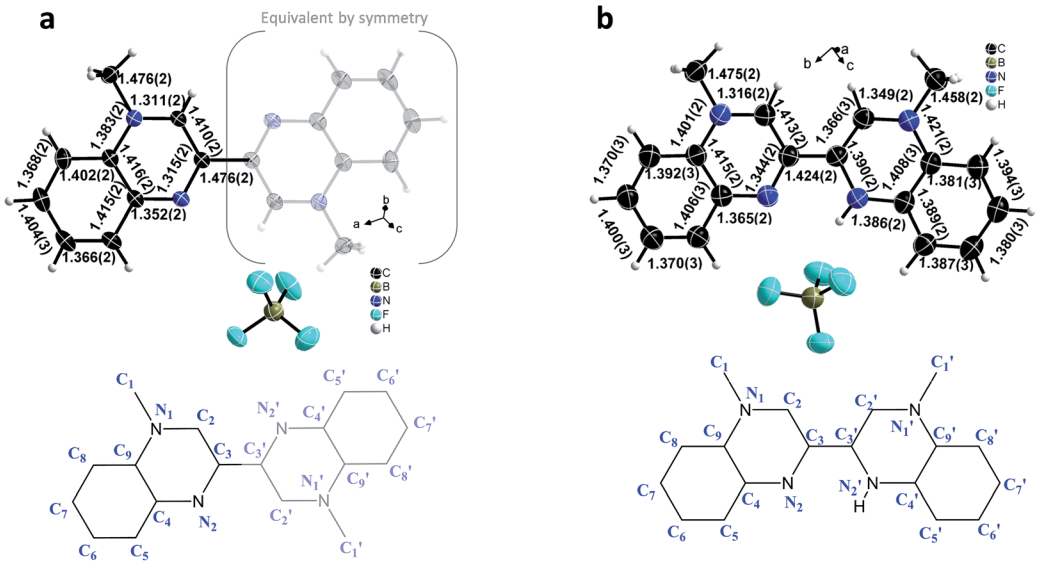

Fig. 2 Crystallographic structures of $1^{2+}/1^{0}$-H^{+}: view of the asymmetric unit of $[MBqn^{2+}](BF_4)_2$, $[1^{2+}](BF_4)_2$ (a) and $[MBqn^{0}$-$H^{+}]BF_4$, $[1^{0}$-$H^{+}]BF_4$ (b). Salient C–N and C–C bond lengths are indicated.

data and refinement results are listed Table 1. Datasets for both structures were collected at 180 K. They were refined in the space groups $P\bar{1}$ for $[1^{2+}](BF_4)_2$ and $[CdCl_2(1^{0})]$, and $P2_1/n$ for $[1^{0}$-$H^{+}]BF_4$. All atoms including hydrogens were identified from Fourier difference maps. All atoms occupy general positions.

The crystallographic asymmetric units of the structures of $[1^{2+}](BF_4)_2$ and $[1^{0}$-$H^{+}]BF_4$ are shown in Fig. 2. The asymmetric unit of $[1^{2+}](BF_4)_2$ contains one independent half $[MBqn^{2+}]$ (1^{2+}) (*N*-methylquinoxalinium MQ^{+} type) and one independent ordered BF_4^{-}. On the other hand, the asymmetric unit of $[1^{0}$-$H^{+}]BF_4$ contains one independent $[MBqn^{0}$-$H^{+}]$ $(1^{0}$-$H^{+})$, as well as one independent ordered BF_4^{-} per compound.

In the case of 1^{0}-H^{+}, after several attempts with different crystals and from different batches, the refinement is such that equal and significant residual electron density peaks (0.4–0.6 e $Å^{-3}$; background 0.18 e $Å^{-3}$) are clearly and systematically located on all aromatic and methyl hydrogen sites, as for 1^{2+}, but with an additional peak close to the nitrogen on 2′ position (Fig. 3, full explanation in the ESI Tables S1–S3†).

Thus for 1^{0}-H^{+}, because 17 H-atoms are clearly present in the molecule, the latter has to be doubly reduced in order to match the singly positive charge balanced by one BF_4^{-}. This can be also viewed as the monoprotonated dication (leading to a 16 + 1 = 17H atoms trication) which was further reduced by two electrons to give the so-called direduced monoprotonated cation 1^{0}-H^{+}.

Complementary FAB and MALDI-TOF mass spectrometry measurement performed on crystals of $[1^{0}$-$H^{+}]BF_4$ are reproducible and in agreement with a single species, differing only by one H-atom either in solution (FAB) or in the solid state (MALDI) (Fig. S5 and S6†). In particular the MALDI spectra in SM matrix shows a clear difference in peak intensity between the 16 H-atoms and 17 H-atoms (m/z = 288.3 and 289.3) which can be assigned as originating from the molecular entities 1^{2+} and 1^{0}-H^{+}.

As a result of the rotational freedom around the central C_3–C'_3 bond, 1^{2+} and 1^{0}-H^{+} could adopt any geometry between planar *trans*- (ϕ = 180°) and planar *cis*- (ϕ = 0°), where the dihedral angle is defined as $\phi = C_2$–C_3–C'_3–C'_2. What we observe is that for 1^{2+} the geometry is exactly planar *trans*, whereas for 1^{0}-H^{+} it is nearly planar *cis* (ϕ = 2.5°).

In the dication 1^{2+}, constituted of two equivalent MQ^{+} moieties, the structure reveals an aromatic π-conjugated system. The average C–C bond length in the benzene ring [1.392(3) Å] corresponds to the intermediate C–C distance of 1.39–1.40 Å observed in a benzene molecule with electron delocalization.[22] In the pyrazinium moiety, the aromaticity is confirmed by the values of the C–C and C–N bond distances, in the range 1.410(2)-1.416(2) Å and 1.311(2)–1.383(2) Å respectively, that are comparable to those found in the literature.[23] The pyrazinium structure is particularly clear on the 1,2,3,4 atomic positions, as shown by the two shortest distances N_1–C_2

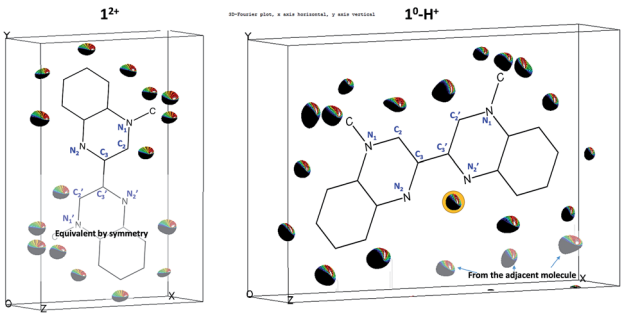

Fig. 3 Scheme of the C,N skeleton of the molecules overlaid with the residual 3D-Fourier difference map of 1^{2+} (left) and 1^{0}-H^{+} (right). For each 1^{2+} and 1^{0}-H^{+} an equal and significant residual electron density is clearly and systematically located on all aromatic and methyl hydrogen sites, as well as a on the nitrogen on the N'_2 position for 1^{0}-H^{+} (highlighted with the yellow circle).

[1.311(2) Å] and N_2–C_3 [1.315(2) Å], alternating with an intermediate length for C_2–C_3 [1.410(2) Å] (Fig. 2).

In contrast, in the direduced monoprotonated cation $\mathbf{1^0}$-$\mathbf{H^+}$ the different redox state of the species and the protonation of only one side of the molecule gives rises to an asymmetric environment. On one hand, the non-protonated MQ moiety remains essentially similar to $\mathbf{1^{2+}}$, where the bond lengths of both benzene ring and pyrazinium core are comparable (N_1–C_2 [1.316(2) Å], N_2–C_3 [1.344(2) Å], C_2–C_3 [1.413(2) Å]). On the other hand, in the protonated half molecule, although the benzene ring remains aromatic (C–C ~ 1.39 Å), significant changes occur mostly within the pyrazinium core. The structure is such that the N'_1–C'_2, N'_1–C'_9 and N'_2–C'_3 bond lengths increase by 0.038 Å, 0.038 Å, and 0.075 Å respectively with a concomitant 0.044 Å decrease in the C'_2–C'_3 bond distance. The central C_3–C'_3 bond also changes dramatically with a net decrease by 0.052 Å, with 1.424(2) Å for $\mathbf{1^0}$-$\mathbf{H^+}$ and 1.476(2) Å for $\mathbf{1^{2+}}$.

These structural features of $\mathbf{1^{2+}}$ and $\mathbf{1^0}$-$\mathbf{H^+}$ have been investigated by quantum chemical calculations using Turbomole[24] (for details see Experimental section in ESI†). For both compounds geometrical parameters were fully optimized in the gas phase at the PBE0/def2-TZVPP level of theory (Tables S4, S5 and S8†), the PBE0 hybrid functional being known to provide the best estimates for such π-conjugated systems.[25,26] The calculated bond lengths fit well with the experimental data with mean absolute errors (MAE) of 0.0068 Å ($\mathbf{1^{2+}}$) and 0.0071 Å ($\mathbf{1^0}$-$\mathbf{H^+}$), whereas the twist angle of the molecule differs only very slightly for $\mathbf{1^0}$-$\mathbf{H^+}$ ($\phi_{exp} = 2.5°$, $\phi_{calc} = 0°$). For $\mathbf{1^{2+}}$ and $\mathbf{1^0}$-$\mathbf{H^+}$ the frequencies calculations, in addition with a scan of the relaxed potential energy surface along the twist angle (ϕ) for $\mathbf{1^{2+}}$, confirmed that the described structures correspond to the ground state of the molecules (Fig. S9 and S13, Tables S6 and S9†). The HOMO and LUMO of $\mathbf{1^{2+}}$, as well as the HOMO of $\mathbf{1^0}$-$\mathbf{H^+}$ are represented in Fig. 4.

As previously stated by A. di Matteo, "a reduction process increasing or decreasing the electron population, in the bonding or antibonding regions, strengthens or weakens the bonds, which become significantly shorter or longer".[25] Here, by populating the LUMO of $\mathbf{1^{2+}}$ (reduction process), a decrease and increase of the bond length is expected between atoms with bonding and antibonding characteristics respectively. This effect will be even more obvious between atoms where the HOMO and LUMO orbitals exhibit the opposite bonding and antibonding features. Thus focusing on the bipyrazinium core, the experimental parameters clearly show that the chemical reduction of $\mathbf{1^{2+}}$ will lead to a shortening of the C_2–C_3 (C'_2–C'_3) and C_3–C'_3 bond lengths and to an increase of the N_1–C_2 (N'_1–C'_2), N_1–C_9 (N'_1–C'_9) and N_2–C_3 (N'_2–C'_3) bond lengths, both having respectively bonding and antibonding characteristic in the LUMO orbital.

The HOMO of $\mathbf{1^0}$-$\mathbf{H^+}$ and the LUMO of $\mathbf{1^{2+}}$ both exhibit comparable bonds with bonding and antibonding characteristics, which is in line with the above reasoning and the observed bond lengths in $\mathbf{1^0}$-$\mathbf{H^+}$. This also shows that the *trans–cis* isomerization which exists between $\mathbf{1^{2+}}$ (*trans*) and $\mathbf{1^0}$-$\mathbf{H^+}$ (*cis*) has no strong influence on the way the π-orbitals overlap.

However, the N'_2–H situation in $\mathbf{1^0}$-$\mathbf{H^+}$ creates a dissymmetry within the molecule leading to a strengthening of the bonding and antibonding features in the pyrazinium core of the protonated MQ. This results in a partial stiffening of the system, in the sense that the electron density can be rather described as localized and alternate single and double bonds, like in polyene-like structure such as dipyran or dithiopyran.[27,28] The N'_2–H situation also stabilizes the preferential *cis*-form in the solid. It creates a strong intramolecular hydrogen bond between the protonated and non-protonated amines ($N_2\cdots H$–N'_2 ~ 2.25 Å), which is also confirmed by the strong bonding characteristic in the $N_2\cdots H$–N'_2 region (HOMO of $\mathbf{1^0}$-$\mathbf{H^+}$ Fig. 4, detail of H-bonds Fig. S7†). This apparently stabilizes $\mathbf{1^0}$-$\mathbf{H^+}$ and might also act as a template by constraining the *cis*-form, *i.e.* the chelate function of the 2,2′-bipyridine.

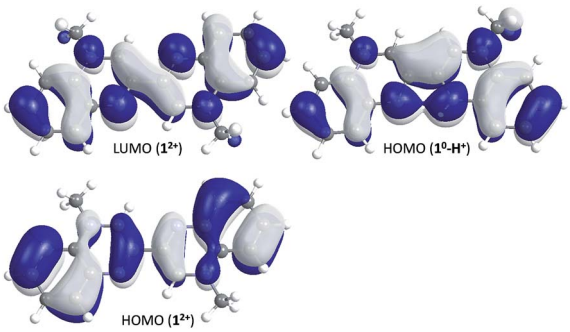

Fig. 4 HOMO and LUMO for $\mathbf{1^{2+}}$ (lower and upper left panel). HOMO for $\mathbf{1^0}$-$\mathbf{H^+}$ (upper right panel).

Spectroscopy, electrochemistry, magnetic susceptibility, spectroelectrochemistry and TDDFT

Because of the poor solubility of $[\mathbf{1^0}$-$\mathbf{H^+}]BF_4$ and in order to get comparative data, both EPR, UV-Vis-NIR, cyclic voltammetry, spectro-electrochemistry, NMR and SQUID experiments have been performed in DMF. Nevertheless, a complementary UV-Vis experiment has been performed in MeCN for $[\mathbf{1^{2+}}](BF_4)_2$ in order to fully identify its electronic transitions below 400 nm.

Electron paramagnetic resonance (EPR) (Fig. 5). A sample of $[\mathbf{1^0}$-$\mathbf{H^+}]BF_4$ dissolved in DMF yielded a 9-line spectrum at ambient temperature. This implies the presence of a paramagnetic species arising from either an impurity or a new redox state in solution. The rich hyperfine pattern could be modelled by coupling the single electron of the doublet radical to the $I = 1$ nuclear spin of all four nitrogen atoms (99.7% natural abundance). This is in line with what is expected for a doublet radical in solution. Simulation yielded spin Hamiltonian parameters $g_{iso} = 2.0069$ and $A_{iso} = 6.05 \times 10^{-4}$ cm^{-1} with a magnitude of the ^{14}N hyperfine coupling comparable to that found for *N*,*N*′-dialkylated quinoxalinium radical cations.[29] The *g*-value is similar to those reported for phosphine-based cation radicals,[30–32] but is slightly higher compared to the methylviologen radical cation (g ~ 2.003).[7,8,33] This is consistent with the extra heteroatom in the six-membered ring hosting the unpaired spin. Consequently, the ^{14}N hyperfine coupling is larger than for the archetypal viologens.[29,34,35]

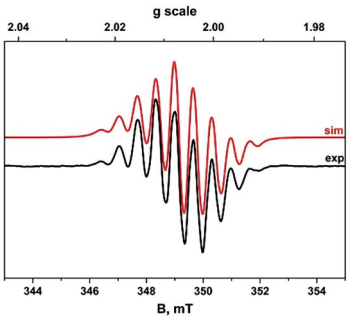

Fig. 5 Isotropic EPR spectrum of the intermediate radical species recorded in DMF solution at 293 K (experimental conditions: frequency, 9.8075 GHz; power, 20 mW; modulation, 0.07 mT). Experimental data represented by the black line and simulation depicted by the red trace.

The absence of additional hyperfine structure from coupling to the methyl and aromatic protons of the organic radical confirms these couplings are less than the isotopic linewidth $\sim 2 \times 10^{-4}$ cm^{-1}, which is invariant irrespective of the measurement temperature. Nevertheless this does not show conclusively whether the paramagnetic species is an impurity or not.

Cyclic voltammetry (CV) (Fig. 6a). In order to gain further insights into the redox process leading to the formation of the paramagnetic species, CV measurements were performed. Furthermore, these were done quantitatively by using the well-known ferrocene/ferrocenium system as internal reference. Regarding its reduction potential (*V vs.* Fc/Fc^{+}), $\mathbf{1}^{2+}$ ($E_{1/2} = -0.54$ V) is an intermediate but strong electron-acceptor between the prototype 3,3′-diazamethylviologen ($DAMV^{\bullet+}$) ($E_{1/2} = -0.35$ V)[19,20,36] and the methylviologen ($E_{1/2} = -0.89$ V).[7] Thus, in two experiments, either the dication $[\mathbf{1}^{2+}](BF_4)_2$ (Fig. 1 – purple) or the doubly reduced monoprotonated cation $[\mathbf{1}^{0}\text{-}\mathbf{H}^{+}]BF_4$ (Fig. 1 – blue) were dissolved in DMF. Both CVs are perfectly reversible and superposable for all investigated scan rates (50–5000 mV s^{-1}).

The deconvolution of the CV allows us to circumvent diffusion problems and to conclude that there is a single-electronic process by comparing with the current peak of the ferrocene/ferrocenium system. This rules out the presence of any impurity and points to the oxidation of the doubly reduced monoprotonated cation $[\mathbf{1}^{0}\text{-}\mathbf{H}^{+}]BF_4$ to give the doublet radical. Furthermore, the voltage separation between current peaks of *ca.* 200 mV is significantly higher than the theoretical value of 59 mV. This is in line with a redox process inducing a significant structural rearrangement such as a *trans–cis* isomerization.[37]

Magnetic susceptibility measurement using SQUID and NMR Evans' method. The magnetic behaviour of the redox states in solid and solution states should also show differences due to the diamagnetic nature of the solid state species $[\mathbf{1}^{0}\text{-}\mathbf{H}^{+}]BF_4$ *versus* the paramagnetic nature of the doublet radical species in solution.

The magnetic susceptibility of $[\mathbf{1}^{0}\text{-}\mathbf{H}^{+}]BF_4$ (Fig. 1 – purple) was measured on a polycrystalline sample over the 4–380 K temperature range under an applied dc field of 1 T. As shown in Fig. S10,† in the solid state the product of magnetic susceptibility with temperature is very close to zero (<0.007 cm^3 K mol^{-1}), which confirms the diamagnetic nature of $[\mathbf{1}^{0}\text{-}\mathbf{H}^{+}]BF_4$ in the solid state.

Furthermore, crystals of $[\mathbf{1}^{0}\text{-}\mathbf{H}^{+}]BF_4$ dissolved in DMF-d^7 under inert atmosphere exhibit a very strong diamagnetism at -5000×10^{-6} cm^3 mol^{-1}, even after correcting with the expected diamagnetic contribution calculated from Pascal constants. Given that we were expecting to see a paramagnetic signature, which would be expected for isolated paramagnetic species, this behaviour suggests the presence of super-diamagnetism. This has been previously observed in 3D inorganic compounds and was coined superdiamagnetism, in an obvious reference to the Meissner effect and the perfect diamagnetism observed in superconductors.[38,39] More recently superdiamagnetism was induced at low temperatures by the application of a magnetic field in a one-dimensional Pt^{II} complex.[40] To the best of our knowledge this has never been observed in a purely organic based compound. In our case the diamagnetic susceptibility reaches 6% of the $1/4\pi$ value expected for complete diamagnetism. This unexpected super-diamagnetism was confirmed using the Evans' ^{1}H-NMR method[41] at room temperature from the strong negative chemical shift of the reference *tert*-butyl alcohol signal at −27.3 Hz in DMSO-d^6 and −25.5 Hz in DMF-d^7 in the presence of our studied molecule (Fig. S11 and S12†). This is typical of an additional diamagnetic environment around the protons of the reference. The calculated magnetic susceptibilities, respectively $\chi = -962 \times 10^{-6}$ cm^3 mol^{-1} and $\chi = -3510 \times 10^{-6}$ cm^3 mol^{-1} are in line with the SQUID measurement, though the effect seems much weaker in DMSO.

This allows us to conclude from the CV, EPR, SQUID and NMR results that a single radical intermediate species is present in solution. Due to the perfect planarity of the molecule (no steric hindrance) and the fact that the spin density is located in π-orbitals, the apparent superdiamagnetic behaviour of such a radical in solution could be tentatively explained from the formation of extended stacks of radicals, in analogy to the unidimensional Pt^{II} complex.[40] Strongly spin-paired π-dimers, as already observed in other π-radicals such as viologen and TTF,[34,42–44] would only provide a "normal" diamagnetic behaviour.

However the question remains: what is the nature of the radical species in solution? In their studies on the prototype *N*,*N*′-dimethyl-3,3′-bipyrazinium dication,[20] and the *N*-methylpyrazinium,[45,46] *N*-methylquinoxalinium[47] and *N*-methylphenazinium[48] cations, Kaim *et al.*, Rouiller & Laviron, Eaton and Takagi *et al.* showed that under mild acidic or neutral conditions the chemical reduction of such kinds of cations is accompanied by protonation thus leading to 4-hydro-1-methyldiazinium 7π electron radical cations in solution. We thus see two possibilities here. Firstly, the dication ($\mathbf{1}^{2+}$) is reduced and isomerises through the addition of an electron to give the *cis*-radical cation ($\mathbf{1}^{\bullet+}$). Secondly, this *cis*-radical cation is formed and further protonated to give the *cis*-protonated radical cation ($\mathbf{1}^{\bullet+}\text{-}\mathbf{H}^{+}$).

In order to investigate this, additional spectroelectrochemical (SE), UV-Vis-NIR and TDDFT experiments were performed. The purpose was to identify a possible structure/optical signature relationship for the three different redox

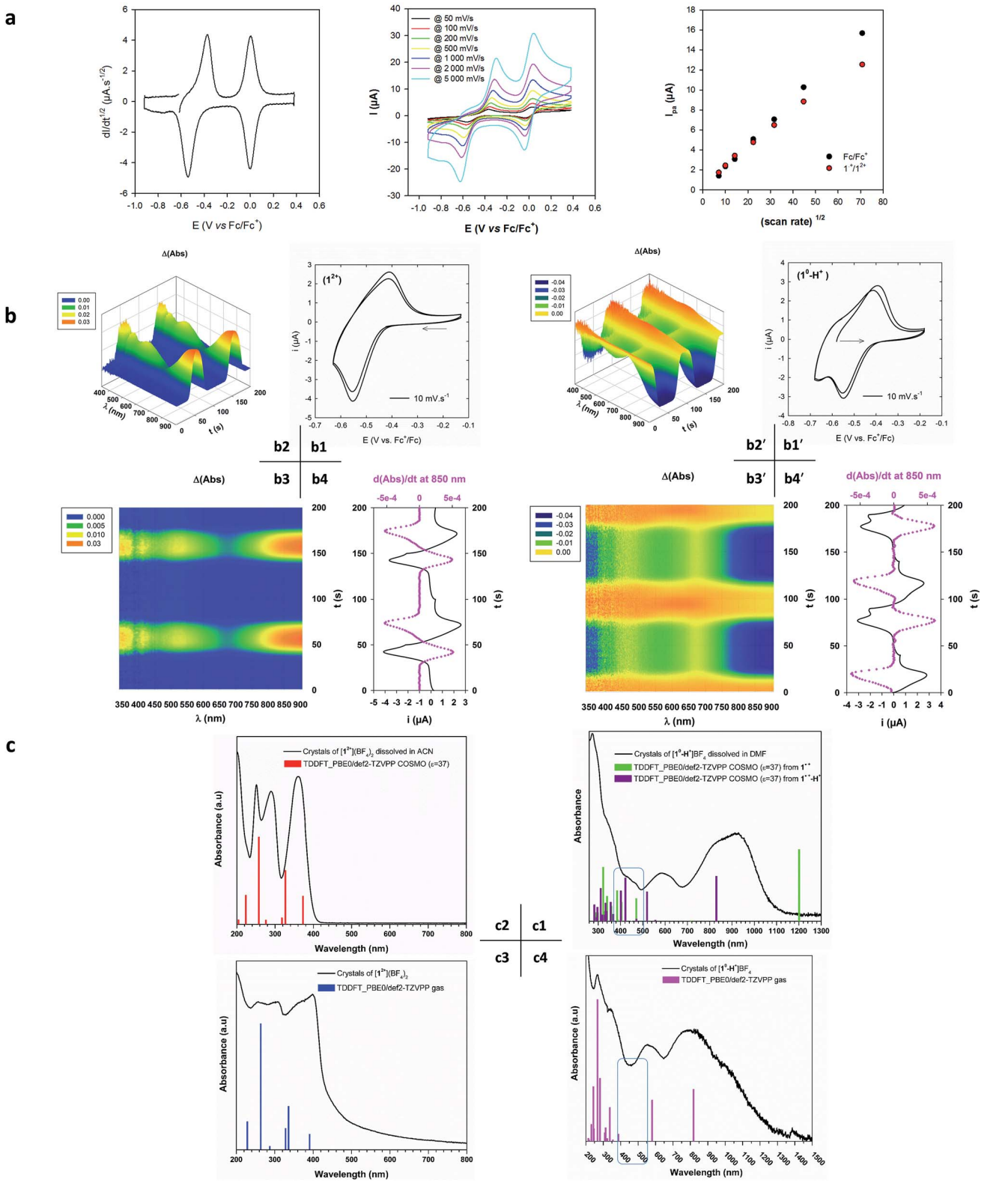

Fig. 6 (a) Deconvoluted cyclic voltammogram (left) $[1^0\text{-}H^+]BF_4$ (0.56 mM) and Fc (0.65 mM) in DMF, with TBAP (0.1 M) as supporting electrolyte on Pt at 200 mV s^{-1}. Evolution of the voltammogram (middle) and the current peak of each redox couple (right) with the variation of the scan rate. (b) Spectroelectrochemistry experiments of 1^{2+} (b) and $1^0\text{-}H^+$ (b′), 0.5 mM in 0.1 M $TBAPF_6$/DMF on platinum electrode, in thin layer conditions (close to 50 μm) under argon at 10 mV s^{-1} and 293 K. (b1 and b1′) CVs in current *vs.* potential representation. (b2 and b2′) 3D representation: (wavelength, time) *vs.* (Δabsorbance). (b3 and b3′) 3D representation viewed along the absorbance axis: (wavelength, time) *vs.* (Δabsorbance). (b4 and b4′) CV and d(Δabsorbance)/*dt* (at 850 nm) *vs.* time, showing a good agreement between the optical and electrochemical data. (c) Overlay of UV-Vis-NIR and TDDFT spectra of 1^{2+} [crystalline state (c3), dissolved in MeCN (c2)], $1^0\text{-}H^+$ [solid state (c4)] and of the intermediate species $1^{\cdot+}\text{-}H^+$ in DMF solution (c1).

states. Optical spectra have been computed using TDDFT at the PBE0/def2-TZVPP level of theory in a closed shell ($\mathbf{1}^{2+}$ and $\mathbf{1}^{0}$-$\mathbf{H}^{+}$) and unrestricted open-shell ($\mathbf{1}^{\bullet+}$ and $\mathbf{1}^{\bullet+}$-$\mathbf{H}^{+}$) configuration. To reproduce the behaviour of the molecules in solution, the conductor-like screening model COSMO has been applied, with $\varepsilon = 37$ as a mean value for a mixture of DMF and MeCN.

Spectroelectrochemistry (Fig. 6(b and b′)). Known to be a powerful tool for analysing the spectral signature of involved species during an electrochemical process, time resolved spectroelectrochemical experiments (SE) were performed, using the already described home-made cell,[49–51] between 350 and 900 nm on dissolved $\mathbf{1}^{2+}$ (Fig. 1 – grey) and $\mathbf{1}^{0}$-$\mathbf{H}^{+}$ (Fig. 1 – purple) (0.5 mM in 0.1 M $TBAPF_6$/DMF), in order to correlate the changes in their spectra during reduction and oxidation processes.

In Fig. 6(b and b′), we see that both voltabsorptograms (Δ(Abs) *vs.* initial species) are perfect mirror images of each other, indicating that the two species are part of the same redox couple. Furthermore, the spectra measured during the SE experiments are quite similar to those obtained by dissolving crystals of $[\mathbf{1}^{2+}](BF_4)_2$ and $[\mathbf{1}^{0}$-$\mathbf{H}^{+}]BF_4$ (Fig. 6c2 and 6c1). The results match perfectly those from the CV in terms of the exclusive presence of one reversible and stable $\mathbf{1}^{2+}/\mathbf{1}^{\mathbf{radical}}$ redox couple in solution.

Solid and solution state UV-Vis-NIR optical properties of the dication $\mathbf{1}^{2+}$. Crystals of $[\mathbf{1}^{2+}](BF_4)_2$ are yellow/off-white in the solid state with no significant absorption in the visible range. The band at $\lambda_{max} = 380$ nm corresponds to the HOMO → LUMO transition (Fig. 6c3, Table S7†). Crystals of $[\mathbf{1}^{2+}](BF_4)_2$ dissolved in MeCN give a colourless solution. The SE spectrum of $\mathbf{1}^{2+}$ exhibits no absorption in the visible region (Fig. 6b), which is confirmed from the UV-Vis spectrum with the lowest energy absorption band slightly shifted compared with the solid state spectrum at $\lambda_{max} = 360$ nm (Fig. 6c2).

Solid state UV-Vis-NIR optical properties of the doubly reduced monoprotonated cation $\mathbf{1}^{0}$-$\mathbf{H}^{+}$. Crystals of $[\mathbf{1}^{0}$-$\mathbf{H}^{+}]BF_4$ are deep purple and absorb across the whole UV-Vis range and well into the near-infrared. There are broad absorption bands centred at 270, 350, 570, 820, and 1000 nm (shoulder ≈1300 nm) (Fig. 6c4). The TDDFT spectrum of $\mathbf{1}^{0}$-$\mathbf{H}^{+}$ matches perfectly with the electronic transitions observed experimentally in the range 200-950 nm, with $\lambda_{max} \approx 820$ nm corresponding to the HOMO → LUMO transitions (Table S10†). Analogous to the behaviour of the methylviologen radical cation either in solution or in the solid state,[7,8] the additional transition present at lower energy is most probably explained due to the formation of extended stacks of $\mathbf{1}^{0}$-$\mathbf{H}^{+}$ species in the solid. This is actually confirmed by the crystal packing which shows an infinite 1D stack of dimers of $\mathbf{1}^{0}$-$\mathbf{H}^{+}$ (Fig. S8†).

Solution state UV-Vis-NIR optical properties of the doublet radical. In the electronic spectrum in solution for a concentration of ≈ 2.4×10^{-4} M the formation of the doublet radical redox state is accompanied by a colour change from the deep purple of the solid to blue with absorption bands centred at 430, 470, 580, 820 and 920 nm (shoulder ≈1100 nm) in the Vis-NIR region (Fig. 6c1). The SE spectrum of the intermediate radical species looks very similar, although the position of the bands is slightly shifted to higher energy by *ca.* 40 nm (0.2 eV) (Fig. 6b).

To investigate the two previously proposed hypothesis, namely (a) the species in solution is a *cis*-radical cation $\mathbf{1}^{\bullet+}$ or (b) the species in solution is the *cis*-protonated radical dication $\mathbf{1}^{\bullet+}$-$\mathbf{H}^{+}$, two different TDDFT spectra were simulated from fully optimized geometries (Tables S12 and S13†).

The TDDFT spectrum corresponding to hypothesis (a) *cis*-$\mathbf{1}^{\bullet+}$ is shown with green lines in Fig. 6c1. This is clearly different from the experimental spectrum in that it exhibits a single broad transition at $\lambda_{max} = 1200$ nm and no transitions between 500 and 1100 nm.

The TDDFT spectrum corresponding to hypothesis (b) *cis*-$\mathbf{1}^{\bullet+}$-$\mathbf{H}^{+}$ is shown with violet lines in Fig. 6c1. The main electronic transitions observed experimentally in the range 400 to 850 nm in the SE spectrum are perfectly reproduced theoretically. The lowest energy band $\lambda_{max} = 820$ nm corresponds to the $^{\alpha}$SOMO → $^{\alpha}$LUMO transition (Fig. 6c1, Table S13†).

This leads us to conclude that the radical intermediate species present in solution is intrinsically composed of the *cis*-protonated radical dication $\mathbf{1}^{\bullet+}$-$\mathbf{H}^{+}$ (Fig. 1 – blue). Furthermore the formation of extended stacks of radicals $\mathbf{1}^{\bullet+}$-$\mathbf{H}^{+}$ in solution is substantiated by the presence of an additional band at lower energy (λ = 920 nm, Fig. 6c1), analogous to the low energy bands observed in aggregated viologens in solution.[7,8]

We also note that although at a first glance the spectra of $\mathbf{1}^{\bullet+}$-$\mathbf{H}^{+}$ (Fig. 6c1) and $\mathbf{1}^{0}$-$\mathbf{H}^{+}$ (Fig. 6c4) look broadly similar, the fact that the spectrum of $\mathbf{1}^{0}$-$\mathbf{H}^{+}$ exhibits no transitions between 400 and 500 nm (Table S10†), provides a rapid fingerprint for the identity of the redox state.

Case of the metal complex $[CdCl_2(\mathbf{1}^{0})]$: chelation and non-Kekulé structure aspect of $\mathbf{1}^{0}$

We provide a first example of a metal complex $[CdCl_2(\mathbf{1}^{0})]$ which illustrates the ability of such a ligand to chelate metal ions (Fig. 7). This proves that the neutral direduced species $\mathbf{1}^{0}$ can be obtained without being protonated unlike in the case of $\mathbf{1}^{0}$-$\mathbf{H}^{+}$, which reinforces the suggestion that the additional proton on N'_2 is labile in solution. In addition, the crystals obtained are air stable, which is important for the further development of robust compounds.

The fact that we were unable to isolate a pure phase of the cadmium complex precluded further characterization.

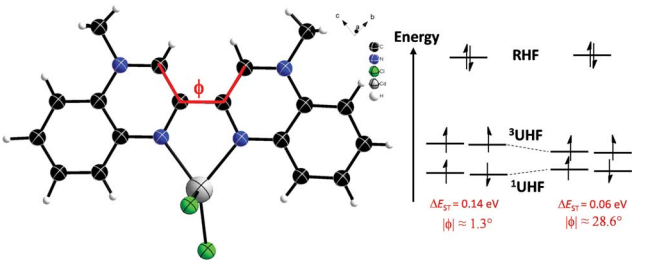

Fig. 7 Thermal ellipsoid view of the asymmetric unit of $[CdCl_2(\mathbf{1}^{0})]$ (left). Corresponding energy level scheme showing the relative energies between singlet RHF, ^{1}UHF and triplet ^{3}UHF, as well as highlighting the open-shell singlet ground state and the ϕ-angle dependent reduction of the singlet to triplet energy gap (ΔE_{ST}) (right) with ϕ the dihedral angle defined by the red lines.

Nevertheless, the reliable crystallographic dataset obtained for this compound has been used as a reference structure for further studies, especially regarding the investigation of the neutral direduced methylbiquinoxen $\mathbf{1^0}$ and its electronic structure.

The asymmetric unit is made of one entire complex [$CdCl_2$($\mathbf{1^0}$)]. The cadmium adopts a distorted tetrahedral coordination environment of D_{2d} symmetry.

The $\mathbf{1^0}$ chelating ligand is *cis*-planar (ϕ = 1.3°) and very symmetric in terms of the relative bond distances (Table S15†). As for $\mathbf{1^0}$-$\mathbf{H^+}$, the multiple bond character of the central C_3–C'_3 bond (d = 1.449 Å) indicates a fully π-conjugated molecule, resulting in a homogenous distribution of the electron density.

Unrestricted DFT calculations for the singlet and triplet state of [$CdCl_2$($\mathbf{1^0}$)] have been performed. The energy of the singlet state is slightly lower than the energy of the triplet state. The energy difference (ΔE_{ST}) amounts to 0.14 eV (Table S14†). However, the ground state shows a significant spin contamination. The analysis of the natural orbitals shows that there is a pair of partly occupied orbitals, one with bonding character between C_3 and C'_3, the other antibonding with occupation numbers of 1.5 and 0.5, respectively, showing partial occupation of the LUMO (Fig. S14†). In addition, the spin density (Fig. S15†) indicates a weakening of the bonding character similar to what is seen in a broken symmetry state. This behaviour is in line with the biradicaloids observed, for example, for under coordinated Sn atoms.[52]

Regarding $\mathbf{1^0}$ in terms of a symmetric and non-protonated structure, not to be confused with the dissymmetric closed-shell monoprotonated cation $\mathbf{1^0}$-$\mathbf{H^+}$, such an open-shell behaviour with a small ΔE_{ST} gap was predictable due to the non-classical (non-Kekulé)[18,20,53,54] electronic structure of $\mathbf{1^0}$, as previously identified by Matheis, *et al.*[18,20] in the prototype molecule, 1,1′-dimethyl-3,3′-bipyrazinium (Fig. S16†). By definition, non-Kekulé means a molecule which is "fully conjugated, but each of whose Kekulé structures contains at least two atoms that are not π-bonded".[55,56] Furthermore, the ΔE_{ST} gap can apparently be significantly reduced by simply twisting the molecule (ΔE_{ST} = $f(\phi)$ Fig. 7), thus giving a means to thermally access the triplet state.

Conclusions and Outlook

As is already known for viologens, the reversible and controllable structural, electronic, and electrostatic changes between the dication and radical species formed in solution invest the $MBqn^{2+/\bullet+}$ redox couple with electron mediation properties. This should be useful for many radical-assisted reactions (photocatalytic H_2 production, C–C bond cleavage, artificial photosynthesis, electrolyte, electrochromism *etc.*).[7,57,58] Surprisingly, chelation to a cadmium centre allowed us to access the direduced solid state biradicaloid species $MBqn^0$ as ligand. Additionally, as expected for such a biradicaloid species, the calculated small singlet to triplet energy gap opens perspectives for a range of exotic electronic, optical, magnetic, dielectric *etc.* properties within a single system composed of purely organic moieties or incorporating metalloid centres. Intriguingly, the superdiamagnetic behaviour observed for the doublet radical species in solution is such an unexpected property for an organic molecule that this demands further investigation.

Acknowledgements

The authors thank the Alexander von Humboldt Foundation (fellowship to N. L) and Helmholtz POF "STN" for financial support. We also thank Christopher Anson and Magali Allain for helpful discussions regarding the crystal structure of the direduced monoprotonated species, Ingrid Freuze for the mass spectrometry measurements, Sven Stahl for the TGA measurements and Lutz Greb for the NMR measurement.

Notes and references

1 W. Kaim and B. Schwederski, *Coord. Chem. Rev.*, 2010, **254**, 1580–1588.
2 P. J. Chirik and K. Wieghardt, *Science*, 2010, **327**, 794–795.
3 A. Heckmann and C. Lambert, *Angew. Chem., Int. Ed.*, 2012, **51**, 326–392.
4 A. C. Fahrenbach, C. J. Bruns, H. Li, A. Trabolsi, A. Coskun and J. F. Stoddart, *Acc. Chem. Res.*, 2014, **47**, 482–493.
5 O. R. Luca and R. H. Crabtree, *Chem. Soc. Rev.*, 2013, **42**, 1440–1459.
6 N. Martin, *Chem. Commun.*, 2013, **49**, 7025–7027.
7 P. M. S. Monk, *The Viologens: Physicochemical Properties, Synthesis, and Application of the Salts of 4,4′-Bipyridine*, Wiley, 1998.
8 T. M. Bockman and J. K. Kochi, *J. Org. Chem.*, 1990, **55**, 4127–4135.
9 N. Mercier, *Eur. J. Inorg. Chem.*, 2013, 19–31.
10 R. J. Mortimer, *Electrochim. Acta*, 1999, **44**, 2971–2981.
11 M.-S. Wang, G. Xu, Z.-J. Zhang and G.-C. Guo, *Chem. Commun.*, 2010, **46**, 361–376.
12 N. Leblanc, M. Allain, N. Mercier and L. Sanguinet, *Cryst. Growth Des.*, 2011, **11**, 2064–2069.
13 A. S. Abouelwafa, V. Mereacre, T. S. Balaban, C. E. Anson and A. K. Powell, *CrystEngComm*, 2010, **12**, 94–99.
14 A. S. Abouelwafa, C. E. Anson, A. Hauser, H. H. Patterson, F. Baril-Robert, X. Li and A. K. Powell, *Inorg. Chem.*, 2012, **51**, 1294–1301.
15 M. Freitag, L. Gundlach, P. Piotrowiak and E. Galoppini, *J. Am. Chem. Soc.*, 2012, **134**, 3358–3366.
16 A. Trabolsi, N. Khashab, A. C. Fahrenbach, D. C. Friedman, M. T. Colvin, K. K. Cotí, D. Benítez, E. Tkatchouk, J.-C. Olsen, M. E. Belowich, R. Carmielli, H. A. Khatib, W. A. Goddard, M. R. Wasielewski and J. F. Stoddart, *Nat. Chem.*, 2010, **2**, 42–49.
17 N. Leblanc, N. Mercier, L. Zorina, S. Simonov, P. Auban-Senzier and C. Pasquier, *J. Am. Chem. Soc.*, 2011, **133**, 14924–14927.
18 W. Kaim and W. Matheis, *Chem. Ber.*, 1990, **123**, 1323–1325.
19 W. Matheis and W. Kaim, *J. Chem. Soc., Faraday Trans.*, 1990, **86**, 3337–3339.

20 W. Matheis, J. Poppe, W. Kaim and S. Zalis, *J. Chem. Soc., Perkin Trans. 2*, 1994, 1923–1928.
21 O. N. Chupakhin, E. O. Sidorov, S. M. Shein and I. I. Bil'kis, *Zh. Org. Khim.*, 1976, **12**, 2464–2468.
22 E. G. Cox, D. W. J. Cruickshank and J. a. S. Smith, *Nature*, 1955, **175**, 766.
23 F. H. Allen, O. Kennard, D. G. Watson, L. Brammer, A. G. Orpen and R. Taylor, *J. Chem. Soc., Perkin Trans. 2*, 1987, S1–S19.
24 TURBOMOLE V6.6 2014, a development of University of Karlsruhe and Forschungszentrum Karlsruhe GmbH, 1989-2007, TURBOMOLE GmbH, since 2007; available from http://www.turbomole.com.
25 A. Di Matteo, *Chem.Phys. Lett.*, 2007, **439**, 190–198.
26 D. Jacquemin, E. A. Perpète, G. E. Scuseria, I. Ciofini and C. Adamo, *J. Chem. Theory Comput.*, 2008, **4**, 123–135.
27 D. Chasseau, J. Gaultier, C. Hauw, R. Fugnitto, V. Gianis and H. Strzelecka, *Acta Crystallogr., Sect. B: Struct. Crystallogr. Cryst. Chem.*, 1982, **38**, 1629–1631.
28 H. R. Luss and D. L. Smith, *Acta Crystallogr., Sect. B: Struct. Crystallogr. Cryst. Chem.*, 1980, **36**, 1580–1588.
29 A. Schulz, W. Kaim and H.-D. Hausen, *J. Chem. Soc., Faraday Trans. 1*, 1988, **84**, 3207–3214.
30 O. Back, B. Donnadieu, P. Parameswaran, G. Frenking and G. Bertrand, *Nat. Chem.*, 2010, **2**, 369–373.
31 X. Pan, X. Chen, T. Li, Y. Li and X. Wang, *J. Am. Chem. Soc.*, 2013, **135**, 3414–3417.
32 X. Pan, Y. Su, X. Chen, Y. Zhao, Y. Li, J. Zuo and X. Wang, *J. Am. Chem. Soc.*, 2013, **135**, 5561–5564.
33 N. Leblanc, N. Mercier, O. Toma, A. H. Kassiba, L. Zorina, P. Auban-Senzier and C. Pasquier, *Chem. Commun.*, 2013, **49**, 10272–10274.
34 A. G. Evans, J. C. Evans and M. W. Baker, *J. Am. Chem. Soc.*, 1977, **99**, 5882–5884.
35 D. W. Clack, J. C. Evans, A. Y. Obaid and C. C. Rowlands, *Tetrahedron*, 1983, **39**, 3615–3620.
36 T. Fujihara, T. Wada and K. Tanaka, *Inorg. Chim. Acta*, 2004, **357**, 1205–1212.
37 N. Terkia-Derdra, R. Andreu, M. Sallé, E. Levillain, J. Orduna, J. Garín, E. Ortí, R. Viruela, R. Pou-Amérigo, B. Sahraoui, A. Gorgues, J.-F. Favard and A. Riou, *Chem.–Eur. J.*, 2000, **6**, 1199–1213.
38 V. L. Ginzburg, *Solid State Commun.*, 1981, **39**, 991–992.
39 V. L. Ginzburg, A. A. Gorbatsevich, Y. V. Kopayev and B. A. Volkov, *Solid State Commun.*, 1984, **50**, 339–343.
40 M. Haruki and P. Wachter, *J. Magn. Magn. Mater.*, 1992, **104–107**, 475–476.
41 D. F. Evans, *J. Chem. Soc.*, 1959, 2003–2005.
42 W. W. Porter and T. P. Vaid, *J. Org. Chem.*, 2005, **70**, 5028–5035.
43 J. M. Spruell, A. Coskun, D. C. Friedman, R. S. Forgan, A. A. Sarjeant, A. Trabolsi, A. C. Fahrenbach, G. Barin, W. F. Paxton, S. K. Dey, M. A. Olson, D. Benítez, E. Tkatchouk, M. T. Colvin, R. Carmielli, S. T. Caldwell, G. M. Rosair, S. G. Hewage, F. Duclairoir, J. L. Seymour, A. M. Z. Slawin, W. A. Goddard, M. R. Wasielewski, G. Cooke and J. F. Stoddart, *Nat. Chem.*, 2010, **2**, 870–879.
44 G.-P. Yong, C.-F. Li, Y.-Z. Li and S.-W. Luo, *Chem. Commun.*, 2010, **46**, 3194–3196.
45 L. Roullier and E. Laviron, *Electrochim. Acta*, 1980, **25**, 795–804.
46 D. R. Eaton, J. M. Watkins and R. J. Buist, *J. Am. Chem. Soc.*, 1985, **107**, 5604–5609.
47 W. Kaim, *Rev. Chem. Intermed.*, 1987, **8**, 247–286.
48 T. Yutaka, A. Kazuyuki, I. Toshiaki, K. Hitomi and I. Kazuhiko, *Chem. Lett.*, 1972, **1**, 847–848.
49 F. Gaillard and E. Levillain, *J. Electroanal. Chem.*, 1995, **398**, 77–87.
50 M. Dias, P. Hudhomme, E. Levillain, L. Perrin, Y. Sahin, F.-X. Sauvage and C. Wartelle, *Electrochem. Commun.*, 2004, **6**, 325–330.
51 O. Alévêque, E. Levillain and L. Sanguinet, *Electrochem. Commun.*, 2015, **51**, 108–112.
52 C. Schrenk, A. Kubas, K. Fink and A. Schnepf, *Angew. Chem., Int. Ed.*, 2011, **50**, 7273–7277.
53 S. Inagaki, *Orbitals in Chemistry*, Springer, 2009.
54 W. T. Borden, H. Iwamura and J. A. Berson, *Acc. Chem. Res.*, 1994, **27**, 109–116.
55 H. C. Longuet-Higgins, *J. Chem. Phys.*, 1950, **18**, 265–274.
56 V. I. Minkin, *Pure Appl. Chem.*, 1999, **71**, 1919–1981.
57 M. D. Forbes, *Carbon-Centered Free Radicals and Radical Cations: Structure, Reactivity, and Dynamics*, Wiley, 2010.
58 P. J. Cappillino, H. D. Pratt, N. S. Hudak, N. C. Tomson, T. M. Anderson and M. R. Anstey, *Adv. Energy Mater.*, 2014, **4**, 1300566.

